Flowfield and Vehicle Parameter Influence on Hypersonic Heat Transfer and Drag

E. V. Zoby* and R. A. Thompson†
NASA Langley Research Center, Hampton, Virginia 23665

A numerical study of several parameters that influence heat transfer, drag, and shock-layer mass-flow rate at laminar and transitional (laminar and turbulent) flow conditions was conducted. The calculations were performed with a detailed computer code, which has been demonstrated to yield excellent comparisons with flight- and ground-test data and with results of other detailed codes. The study focuses the attention of designers of future transatmospheric vehicles on fundamental parameters, such as bluntness and angle of attack, which can have an impact on even initial design and trajectory options. Although the requirement of a reliable transition criterion was not as critical in this study as it obviously would be in aeroheating design studies, the problem of selecting a dependable criterion for the present investigation was evident in this discussion. The effects and trends of the parameters, which also include influence of gas chemistry, are intended to be general in nature, but the information should be of practical use in the design of slender hypersonic vehicles for the ranges of body angle and angle of attack considered in this study.

Nomenclature

C_D = total-drag coefficient
C_{D_f} = skin-friction drag coefficient
C_{D_p} = pressure-drag coefficient
L = vehicle length
M = Mach number
n = shock layer distance from surface
p = pressure
Q = integrated heat-transfer rate
q = heat-transfer rate
Re_θ = momentum thickness Reynolds number
r_n = nose radius
s = surface distance
U_∞ = freestream velocity
X = axial distance
α = angle of attack
γ = ratio of specific heats
θ_c = cone half angle
ϕ = circumferential angle measured from windward centerline
ψ = flow turning angle

Subscripts

e = boundary-layer edge
sh = shock
ref = reference value
w = wall
∞ = freestream condition

Presented as Paper 87-1475 at the AIAA 22nd Thermophysics Conference, Honolulu, HI, June 8-10, 1987; received June 26, 1989; revision received Oct. 16, 1989.

*Aerospace Technologist, Aerothermodynamics Branch, Space Systems Division. Associate Fellow AIAA.

†Aerospace Technologist, Aerothermodynamics Branch, Space Systems Division. Member AIAA.

Introduction

A RESURGENCE in interest to improve both the understanding of viscous flowfield phenomena and the subsequent computational application to hypersonic slender bodies has occurred. The motivation for this change has been the proposed transatmospheric vehicles (TAV).[1,2] The trajectory of a TAV will encompass a large range of freestream conditions. The low altitude conditions require methods capable of predicting reliable laminar and turbulent heating rates in flowfields dominated by perfect-gas or equilibrium-air chemistry. The high altitude conditions require methods that include nonequilibrium chemistry with consideration for shock and surface slip and surface catalytic effects. With the advent of super computers, computational fluid dynamic (CFD) procedures (e.g., Refs. 3-6) for application to complex vehicle geometries have become a reality. Obviously, these methods must be verified with available information prior to use in design studies.

A recent investigation[7] has attempted to demonstrate such a process for a detailed code and several engineering codes. The results of a viscous shock-layer (VSL) method were compared with flight- and ground-test data as well as results of other detailed codes. The comparison of the VSL code results with the available results was good. The VSL equations are a subset of the Navier-Stokes (NS) equations and are valid from the body to the shock. This method provides a useful technique for investigating flowfield technology areas since the VSL method requires much less computer storage and time than other detailed methods. Consequently, studies based on the VSL calculations have been conducted to improve the understanding of several flowfield phenomena for application to slender-body flowfield computations, and the results have been published.[7-10]

The ongoing development of more efficient CFD methods and the study of important technology areas will and should continue. However, there are certain fundamental flowfield and vehicle parameters that can have an impact on the very basic choice of vehicle design or trajectory construction for slender hypersonic vehicles. The influence of such parameters as nose and body bluntness, angle of attack, and flowfield chemistry on the heating or drag are definitely not new. For example, previous studies[11-13] have demonstrated the impact of nose blunting on reducing drag and heat transfer. However, as future TAV missions begin to evolve, it is pertinent to focus

the attention of or possibly inform the present-day vehicle designer on basic available options in vehicle design and trajectory shaping that can affect the heating or drag of a vehicle. In addition, the knowledge of mass-flow rates through the shock layer can be of importance for the TAV that employs air-breathing propulsion. The purpose of the paper is to present detailed VSL solutions over simple geometries to illustrate the effects of blunting and angle of attack on laminar, transitional, and turbulent heating levels. Since the onset and extent of boundary-layer transition are currently based on correlations, the quantitative comparisons, which include turbulent calculations, should be understood to be dependent on the assumed criteria. Corresponding computed results for drag and mass-flow rates are likewise included. The paper provides an insight also to the influence of equilibrium-air and nonequilibrium chemistry on the results. The trends and effects are intended to be general for the range of cone angles and angles of attack considered in this study, and the information should be of practical use to designers. In addition, many of the existing studies were based on approximate prediction techniques that are frequently employed in conceptual and preliminary design studies. The engineer now has the potential to compare the results of the approximate techniques with the detailed results and evaluate the applicability range for the approximate methods. Such a study based on engineering heating methods and simple geometries was recently published.[7]

Analysis

The three-dimensional VSL method is based on the solution in which parabolic approximations are made in both the streamwise and crossflow directions. The VSL equations are obtained by retaining terms in the NS equations up to the order of the inverse square root of the Reynolds number. In the VSL method, the entire shock layer is modeled with a single set of equations that are valid through the inviscid and viscous regions and thereby eliminate inherent difficulties encountered in matching boundary-layer and inviscid solutions, e.g., accounting for entropy effects. Davis[14] developed the application of the VSL equations for two-dimensional flows over axisymmetric configurations. Murray and Lewis[15] extended the method to three dimensions and applied their code (VSL3D) to spherically blunted conical configurations. The VSL3D code was then modified[16] to include transition and turbulent flow and the capability for treating air in chemical equilibrium. A further extension[17] of the code was made wherein the chemistry modeling was changed to treat chemical nonequilibrium in the shock layer. With some additional modifications,[18,19] the two later versions[16,17] of the VSL3D code are used in this paper. Also, for the present study, the Cebeci-Smith[20] turbulence model includes the method of Gupta et al.[9] for the pressure gradient term.

A basic limitation of the VSL procedure is the inability to compute through flow regions characterized by separation, e.g., crossflow separation over the leeward region of vehicles at angle of attack. This situation has been encountered even for long bodies at small angles of attack. However, the prediction of the aerothermal windward environment has been demonstrated[7] to produce accurate results.

The basic governing equations, the thermodynamics and transport properties, the turbulence modeling, the boundary conditions, the chemical kinetics, and the method of solution are presented in detail in Refs. 15–19. This paper does not repeat these thoroughly documented topics.

Results and Discussion

In this section, results of the numerical study are presented. Since the present calculated values are based on a VSL code that has been shown[7] to yield excellent comparisons with flight- and ground-test data and with results of other detailed codes, the predictions can be considered quantitatively as well as qualitatively reliable. The predicted results illustrate the effects of fundamental parameters, such as bluntness and angle of attack, on the heat transfer, aerodynamic forces, and transition for simple slender hypersonic vehicles. The influence of gas chemistry is also demonstrated. In addition, the effects of these parameters on the shock-layer mass-flow rates are discussed. The impact of these parameters on the surface-measurable quantities has been previously predicted by engineering or empirical methods, and the VSL code provides a mechanism to evaluate the range of applicability of approximate methods. In this study, the computed heating rates are nondimensionalized by an arbitrarily selected heating rate for each figure. The present effects and trends are general in nature. However, the information may be of practical use to the designer of present or future slender hypersonic vehicles by simply focusing attention on the basic options that can affect vehicle design or trajectory construction.

Nose-Bluntness Effects

The concept of nose blunting to minimize drag and heating rates is not new, and studies[11–13] have demonstrated the benefits. The optimum nose bluntness can be based on drag and heating parameters as well as many others, for example, volume, stability derivatives, or flowfield effects such as pressure losses and mass-flow capture. Also, the optimum shape may depend on freestream conditions, such as Reynolds number, as was shown in Ref. 12. In this paper, the intent is to illustrate effects or trends of a parameter on the heating, drag, and so forth, and not to determine an optimum shape.

Two vehicles, with nose radii of 0.125 and 0.75 ft and angles of attack of 0, 3, and 20 deg, were considered for this phase of the study. The axial length of the smaller nose radius body was selected as 140 ft. Blunting was accomplished by keeping the cone angle and base radius fixed and increasing the nose radius. Although this blunting results in a physically shorter body ($\simeq$ 135 ft) with smaller volume, these changes are a small fraction of the total vehicle size. Detailed calculations (VSL3D) were made for a freestream Mach number of 15 at 150,000 ft altitude. (Comparison of detailed and engineering code predictions are presented in Ref 7.) Both fully laminar and transitional (laminar and turbulent) flow were computed for the zero-lift case while only transitional solutions were obtained for the angle-of-attack cases. For the turbulent heating cases, presented in Ref. 7, boundary-layer transition locations were computed using the VSL3D code with the Re-entry-F transition correlation[21] and a transition zone model as described in Ref. 22. The transition correlation was developed with the experimentally determined Re-entry-F transition locations and the approximate flowfield codes available in the late 1960s. First, note that the predicted transition locations with the VSL code and the Re-entry-F experimentally determined locations were stated in Ref. 7 to be in good agreement. Second, for the Re-entry-F conditions, the computed flow conditions at the locations predicted by the VSL3D code with the correlation did yield a reasonably good comparison ($\leq$ 20%) with other transition criteria, such as a ratio of $Re_\theta/M_e = 150$. The flow conditions were assumed to be defined by the edge of the thermal boundary layer in the VSL3D calculations as discussed in Ref. 7. These two results are not necessarily surprising since the comparisons were generally made at conditions representative of sharp-cone flow. However, a 20% deviation in the Re_θ/M_e ratio can result in large differences in the predicted and actual transition location for some flow conditions. For this study, the predicted results were used only to illustrate the effect of the parameters on transition movement and do not reflect an attitude of the investigators on the actual occurrence of boundary-layer transition. Recognize that relative comparisons of quantitative results that are based on an assumed transition criterion can be affected by the assumed correlation and the transition zone model. The Re-entry-F correlation has not been used to the knowledge of the authors in comparison with experimentally determined transition locations for other vehicles and flow conditions. In the current calculations, a constant wall temperature of 2260 °R was used,

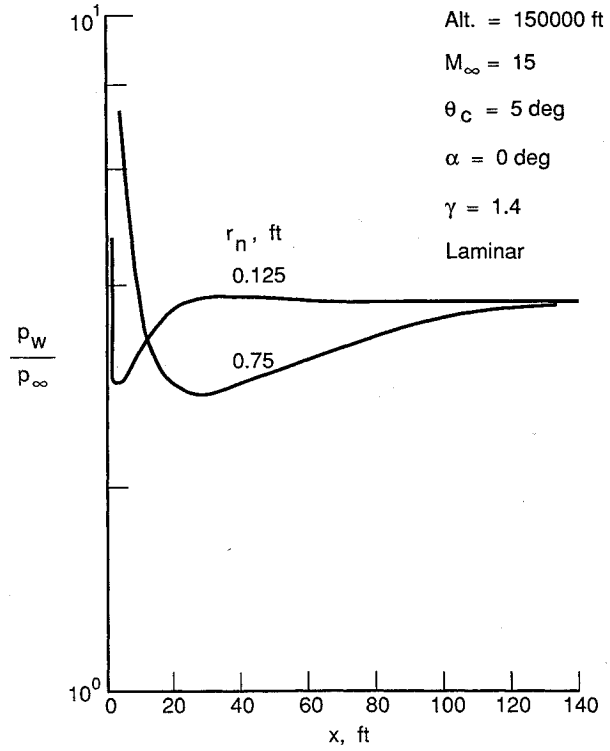

Fig. 1 Surface-pressure distributions.

Table 1 Predicted drag coefficient and heating on the 5-deg cone at $M_\infty = 15$, $\alpha = 0$ deg, $\gamma = 1.4$

r_n, ft	C_{D_P}	C_{D_f}	C_D	Q, Btu/s
	(a) Laminar			
0.125	0.01771	0.00472	0.02243	9800
0.75	0.01856	0.00358	0.02213	8390
	(b) Transition			
0.125	0.01885	0.01687	0.03572	35070
0.75	0.01940	0.01078	0.03018	23990

and perfect-gas chemistry was assumed throughout the shock layer. The neglect of real-gas properties for these nose-bluntness calculations will be shown in a later discussion to have no influence on the trends.

The predicted surface pressure distributions over the 5-deg cone with laminar flow are shown in Fig. 1 for both nose radii. The pressure over the smaller nose-radius body is dominated by the nose for the first 25 ft only. Downstream, the pressure is constant and equal to sharp cone pressure. In contrast, the pressure on the blunter body is completely influenced by the nose and is lower over most of the afterbody. The pressure-drag coefficients computed by integration of the distributions in Fig. 1 are presented in Table 1(a). As expected, the pressure-drag coefficient increased as the nose radius was increased for the fixed cone angle and base radius. However, even with a factor of 6 increase in nose radius, the resulting increase in pressure drag was relatively small as a result of the lower pressure over the body length. Furthermore, when laminar frictional forces are included, the skin-friction drag and, consequently, the total drag [Table 1(a)] are lower on the blunter cone. A similar reduction in skin friction was demonstrated by Moeckel[13] for flat plates with bluntness.

Coupled with the benefit of reduced drag coefficient, increasing nose bluntness also reduces stagnation and afterbody laminar heating. These expected results are shown in Fig. 2. A parameter that is useful in a comparative study and in vehicle thermal design is the total heating rate to the vehicle surface. These results, which were calculated by integrating the heating distributions (Fig. 2), are presented in Table 1(a) and indicate a 15% decrease in the total heat load for the larger nose radius cone.

The effects of transition on the previous laminar results were investigated and are also shown in Fig. 2 and Table 1(b). In general, the trends are the same as for the laminar results except the magnitudes of the decrease in drag and heating with bluntness are larger. For example, the total drag coefficient on the 0.75-ft nose radius cone is 15% less than for the smaller nose radius (0.125 ft) cone, and the corresponding integrated heating is 30% less. These larger decreases are primarily due to the rearward movement of transition with increased bluntness. In Fig. 2, increasing bluntness is shown to move the transition location rearward by about 25 ft. Although this transition-front behavior with increasing bluntness has been demonstrated experimentally,[23,24] the transition locations that are shown in Fig. 2 are possibly questionable since flow conditions at these locations that were predicted with the Re-entry-F correlation do not fit other transition criteria that would predict transition farther downstream in both cases. For example, at the transition locations shown in Fig. 2, the local conditions would result in Re_θ/M_e ratios of 54 and 75 for the 0.125 and 0.75-ft nose radii cases, respectively. These values are much lower than those generally employed for a transition criterion. Nevertheless, the trends due to bluntness for either criterion are in agreement.

Angle-of-Attack Effects

Integrated heating results for the nose bluntness and angle-of-attack (AOA) ranges used in the first phase of this study are

Table 2 Integrated heating rates on windward surface, -90 deg $\leq \phi \leq 90$ deg, of the 5-deg cone for $M_\infty = 15$, transition, $\gamma = 1.4$

	Q, Btu/s		
r_n, ft	$\alpha = 0$ deg	$\alpha = 3$ deg	$\alpha = 20$ deg
0.125	17534	24832	80830
0.75	11995	22908	—

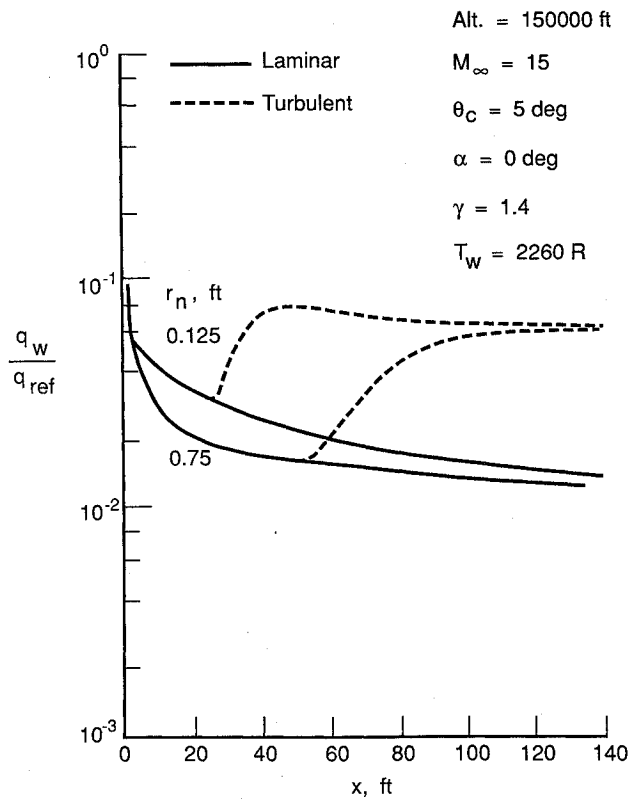

Fig. 2 Laminar and transitional heat-transfer distributions.

summarized in Table 2, and the heating distributions for both nose bluntnesses at 3-deg angle of attack are shown in Fig. 3. This figure compares the predicted windward ($\phi = 0$ deg), side ($\phi = 90$ deg), and leeside ($\phi = 140$ deg) laminar and turbulent heating distributions. One point of interest is the transition locations computed with the Re-entry-F correlation. Transition was computed to be more forward on the windside than on the leeside. This result was also observed in the Re-entry-F experimental transition data.[25] Furthermore, some ground-test experimental data[26-31] for blunted cones with similar ratios of angle of attack to cone half-angle exhibited this behavior. In addition, the transition location on either side was predicted, as in the 0-deg AOA case, to move rearward with increasing bluntness. The results demonstrate again the benefits to be gained by nose blunting, i.e., reducing laminar heating rates and, at least for the conditions of this study, delaying transition.

Since a complete leeside flowfield could not be computed, the total heating loads given in Table 2 represent the integrated heating rates to the windward surface only ($-90 \le \phi \le 90$ deg). The heating loads for both vehicles at the 3-deg AOA condition differ by less than 10%; although increasing bluntness was shown to decrease the laminar rates and delay transition at the 0-deg AOA condition. This result is obtained because the turbulent rates are of the same magnitude regardless of blunting and persist over regions of the vehicles with the largest surface area. The location of transition onset can obviously impact this result. An interesting observation of the heating distributions shown in Fig. 3 is that the heating reduction due to nose blunting along a given meridional plane increases from the windward to leeward side and is due primarily to the increasing extent of the transition region. This observation can be impacted not only by the transition onset but also by the transition zone model. At 20-deg angle of attack, the heat load is shown to be greater than a factor of three times the corresponding value at 3-deg angle of attack for the small nose radius case, but detailed results were not calculated for the bluntest vehicle. Throughout this discussion, the impact of a boundary-layer transition criterion is evident, and the requirement for a reliable transition criterion for future parametric or design studies is clearly demonstrated. In the past, this problem was addressed by using probably very conservative estimates for the onset of transition and more than likely resulted in over-designed thermal protection systems. However, for the high performance transatmospheric vehicles to accomplish their missions, conservatism in the design procedure needs to be reduced.

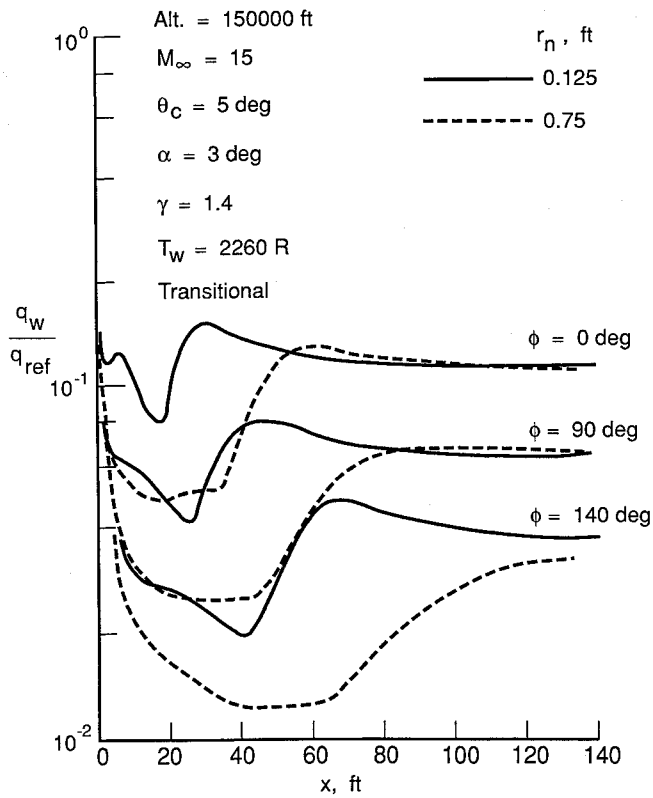

Fig. 3 Heat-transfer distributions at angle of attack.

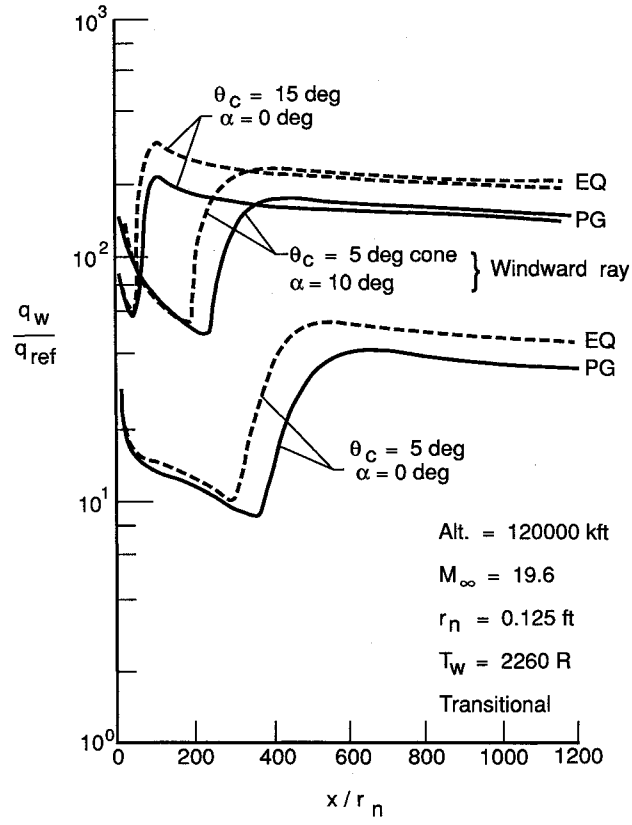

Fig. 4 Effect of gas chemistry and angle of attack on heat-transfer levels.

The second phase of the study includes the effects of nose and body bluntness and angle of attack with equilibrium-air calculations on the heat transfer and drag. Since the previous computed transition locations based on the Re-entry-F correlation were significantly different from locations that would be obtained with an "accepted" Re_θ/M_e criterion, the comparisons shown in Fig. 4 and for the remainder of this study are based on an Re_θ/M_e ratio of 150. This value was not adjusted for any parameter considered in this study, e.g., angle of attack, and the transition trends, therefore, simply reflect the influence of flow property variation Re_θ/M_e. In Fig. 4, results of predictions that illustrate both angle-of-attack and gas-chemistry effects on the laminar and turbulent heating levels and on the computed transition location are shown. The predictions are based on a 5-deg cone with a 0.125-ft nose radius at an altitude of 120,000 ft and a Mach number of 19.6. For the 5-deg cone, calculations are presented at 0- and 10-deg angle of attack for both perfect-gas and equilibrium air conditions. In addition, calculations are shown for a 15-deg cone at 0-deg angle of attack to illustrate possible discrepancies resulting from use of an equivalent cone to predict heating levels and transition location for the 5-deg cone at 10-deg angle of attack. The assumption of an equivalent body condition is used often in preliminary design and parametric studies to model a vehicle at angle of attack. This assumption obviously requires less computational time, but the reliability of the resulting values needs to be understood.

For the 5-deg cone at both 0- and 10-deg angle of attack, the equilibrium-air laminar heating rates are shown to be approximately 10% greater than the perfect-gas results whereas the

Table 3 Predicted drag coefficient and heating with transition at altitude = 120,000 ft, $M_\infty = 19.6$, $\alpha = 0$ deg, and $r_n = 0.125$ ft

θ_c, deg	C_{D_P}	C_{D_f}	C_D	Q, Btu/s
	(a) Perfect gas			
5	0.01823	0.01089	0.02911	201160
15	0.14308	0.01568	0.15876	2609630
	(b) Equilibrium air			
5	0.01826	0.01456	0.03283	270890
15	0.14217	0.02128	0.16345	3637100

Table 4 Integrated transitional heating rates for -90 deg $\leq\theta\leq$ 90 deg over 5-deg cone with $r_n = 0.125$ ft at altitude = 120,000 ft and $M_\infty = 19.6$

	Q, Btu/s	
α, deg	Perfect gas	Equilibrium air
0	100580	135440
10	143140	198340

corresponding turbulent comparisons produce a 30% increase. However, note that boundary-layer transition is computed at about the same body location for the equilibrium-air or perfect-gas condition. Also, for an increasing angle of attack, a forward movement of the transition location on the windward ray is computed for both perfect and real-gas chemistry conditions. The forward movement of transition on the windward side with angle of attack was also obtained in some ground-test experimental transition data[26-31] on slightly blunted slender cones.

The laminar heating rates for the 5-deg cone at angle of attack are shown to be significantly higher than the rates based on the equivalent cone case (15-deg cone at 0-deg AOA). This result is noted for equilibrium-air or a perfect-gas condition and is due to the effects of crossflow on a laminar flowfield solution. However, for either perfect or equilibrium-air gas calculations, the turbulent levels for the cone at angle of attack and for the equivalent-cone case are essentially the same, and these trends have been noted previously in the literature.[32,33] Also, the results of Fig. 4 show that the computed transition location for the equivalent cone yields a very conservative prediction relative to the value for the 5-deg cone at angle of attack as might be expected.

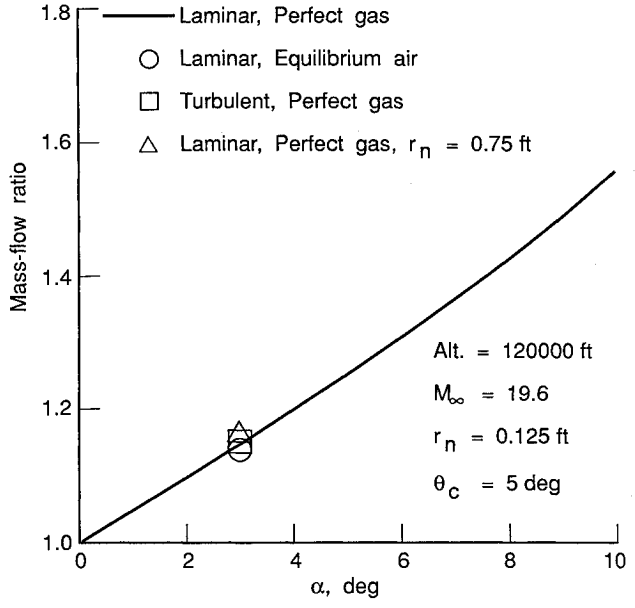

Fig. 5 Angle-of-attack effects on mass-flow ratio at $x = 100$ ft.

A summary of the two 0-deg AOA cases for aerodynamic forces and integrated heating are presented in Table 3. As expected, the pressure-drag values for a given cone angle are essentially the same with perfect-gas or equilibrium-air assumptions. The larger skin-friction drag and total integrated heating equilibrium-air values are reflected by the higher turbulent heating-rate levels shown in Fig. 4. However, the total drag values for perfect-gas and equilibrium-air calculations for either cone angle do not show as large of an increase as the comparisons presented for skin-friction drag results (>30%). The total drag results are pressure dominated, especially for the larger cone angle. However, the increase of approximately 35% in total heating values for equilibrium air could easily present design considerations.

Total heating loads illustrating angles-of-attack and gas-chemistry effects are presented in Table 4. Since a complete flowfield solution was not possible, the total heating loads represent integrated heating rates from $-90\leq\phi\leq 90$ deg, and the 0-deg AOA values are based on the same range. A comparison of the 10-deg angle of attack to 0-deg heating loads yields a factor of approximately 1.45 for either perfect or equilibrium-air gas conditions, and a comparison based on equilibrium to perfect-gas results for either AOA condition produces ratios of approximately 1.35.

Finally, the effects of angle of attack, gas chemistry, and flow conditions on the shock-layer mass-flow rates are discussed. The integrated mass-flow rate at a given location on a TAV configuration is an important factor in air-breathing propulsion design. Shock-layer mass-flow rates have been computed at a body station of 100 ft on a 5-deg cone with a 0.125-ft nose radius. The computed results have been obtained over a range of angles of attack from 0 to 10 deg for perfect-gas or equilibrium-air chemistry and for all laminar flow or transition-to-turbulent flow conditions. The influence of bluntness was also considered. The results are presented in Fig. 5 in terms of a mass-flow ratio as a function of angle of attack. The ratio is the integrated mass flow through the shock layer at a given angle of attack to the laminar, perfect-gas 0-deg AOA value. The mass-flow values are integrated shock-layer rates from -90 deg $\leq\phi\leq 90$ deg. The variation in boundary-layer and gas-chemistry states and increased nose bluntness were determined to have only a small effect on the ratio at the 3-deg AOA condition as shown in Fig. 5. At the

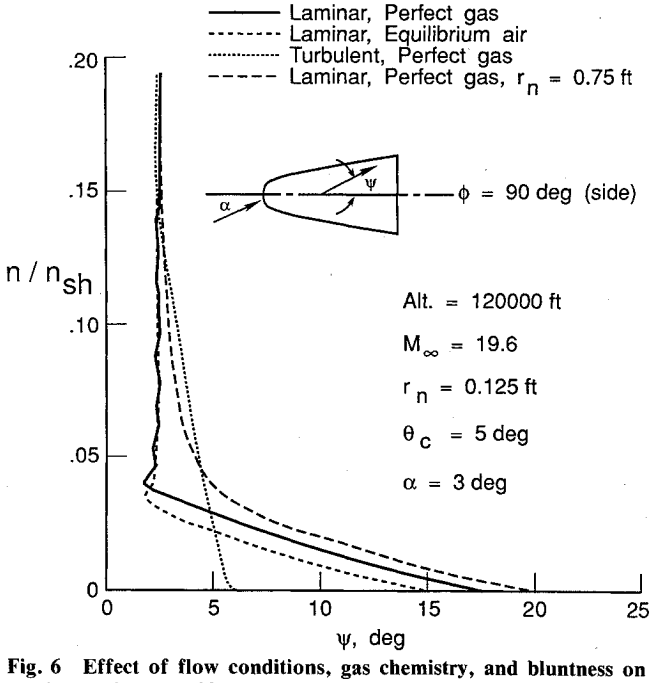

Fig. 6 Effect of flow conditions, gas chemistry, and bluntness on turning angle at $\phi = 90$ deg and $x = 100$ ft.

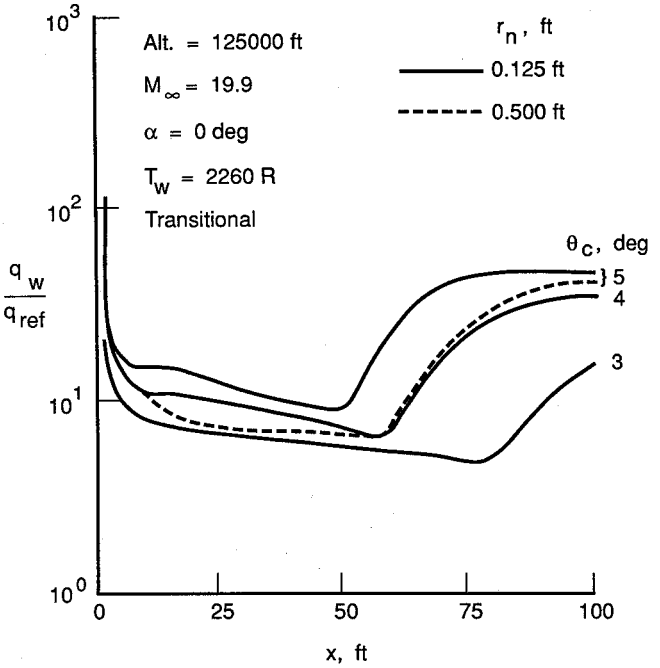

Fig. 7 Bluntness effects on equilibrium air heat-transfer distributions.

10-deg AOA condition, the mass flow at the 100-ft body station is approximately 55% larger than the corresponding value at 0-deg angle of attack and is due to a greater cross-sectional area of the shock layer at angle of attack compared to the 0-deg condition.

For these calculations, the only apparent negative impact that angle of attack may have on the windward surface mass flow is illustrated in Fig. 6. This figure presents the flow turning angles through the shock layer at the 90-deg (side) meridian and the 100-ft station. The 90-deg meridian represents the location of maximum turning between -90 deg $\leq\phi\leq$ 90 deg. The calculated values are based on a 3-deg AOA value, and they illustrate the influence of turbulence, gas chemistry, and bluntness of the magnitude and distribution of the flow turning angle through the shock layer. For all the calculations, the outer 85% of the shock layer experiences a flow turning angle ψ of approximately 2.5 deg, which is less than the angle of attack. For the laminar perfect-gas and equilibrium-air cases based on a nose radius of 0.125 ft, only the inner 5% of the shock layer, which corresponds to the viscous region for these calculations, experiences flow turning angles greater than 2.5 deg. However, turning angles greater than 2.5 deg are shown for the turbulent flow case and the laminar flow calculation with increased bluntness ($r_n = 0.75$ ft) over the inner 15% of the shock layer. The turbulent flow results are due to viscous effects that are encountered at a greater distance from the surface ($n/n_{sh} = 0$) than the corresponding laminar condition. For the larger nose radius condition, the flowfield has not completely recovered to sharp-cone conditions (see Fig. 1), and influences on the flow turning angle extend slightly into the inviscid flow region. Therefore, at large downstream distances, the large crossflow effects attributed to conical flow configurations are apparently influential only in the near-wall viscous-flow region. Crossflow is known to significantly affect local laminar heating and shear, and the effect is exemplified in the turning angles computed for the laminar-flow conditions presented in Fig. 6. Turning angles at the surface are shown to be as large as 15 to 20 deg. Likewise, crossflow is known to have a smaller effect on the turbulent heating level, which is corroborated by the smaller turning angle of approximately 6 deg.

Cone-Angle Bluntness Effects

Additional computed results for the effect of small cone angles on the equilibrium-air transitional and turbulent heating rates are shown in Fig. 7. The heating-rate distributions are presented over cone angles of 3, 4, and 5-deg with a 0.125-ft nose radius. For these shapes, the length was held constant and the base radius was changed. The associated aerodynamic forces and total heating loads are presented in Table 5. An altitude of 125,000 ft with a Mach number of 19.9 was used in this set of calculations. A calculation for a 5-deg cone with a 0.5-ft nose radius is also presented to demonstrate that the perfect-gas nose-blunting trends that are shown in Fig. 2 and Table 1 are not altered for equilibrium conditions. The results presented in Fig. 7 illustrate that an increasing trend for cone angle produces a forward movement of boundary-layer transition. Significant differences in boundary-layer transition locations and heating-rate levels are observed by increasing the cone angle from 3 to 4 deg compared with the 4 to 5 deg change. These differences are reflected in the total heating and

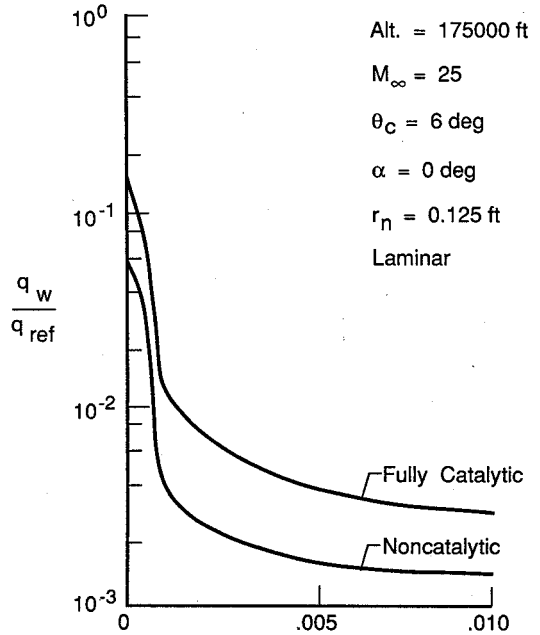

a) Fore cone

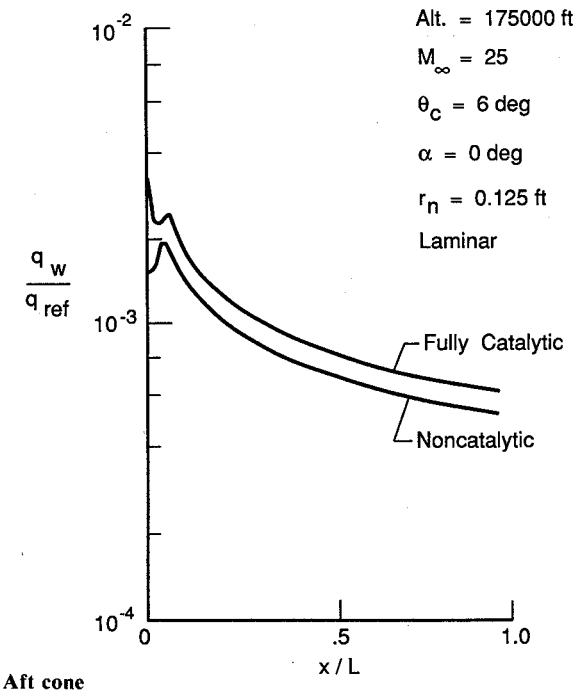

b) Aft cone

Fig. 8 Nonequilibrium heat-transfer predictions.

Table 5 Equilibrium-air predicted drag coefficient and heating with transition at altitude = 125,000 ft and $M_\infty = 19.9$, $\alpha = 0$ deg, and $r_n = 0.125$ ft

θ_c, deg	C_{D_P}	C_{D_f}	C_D	Q, Btu/s
3	0.00708	0.00467	0.01175	17270
4	0.0121	0.00945	0.02156	51290
5	0.01835	0.01223	0.03058	92430

drag values of Table 5. Incremental changes in cone angle are observed to increase significantly the total heating in comparison to the results of Table 2 for similar increments in angle of attack.

Nonequilibrium Effects on Heating

A calculation was performed for this study to illustrate the magnitude of the effects of nonequilibrium chemistry on heat-transfer rate for a slender body at 0-deg angle of attack. In this VSL solution, a 6-deg sphere cone with a 0.125-ft nose radius was used. Freestream conditions were selected at 175,000 ft and a Mach number of 25. Both noncatalytic and fully catalytic surfaces were examined to show the limiting effects of wall catalycity on heating. The predicted heat-transfer distributions are shown in Figs. 8a and 8b. The first of these figures is an enlarged view of the nose region, whereas the second covers the full length. The important result in these figures is that the heating is 50% less than noncatalytic surface results to the fully catalytic results over the nose region and extending downstream about 1% of the body length. The present calculations show that farther aft the decreases in heating are much less (about 15%). Also, the differences shown in the figure were obtained for theoretical boundary conditions. Some degree of catalysis is usually present for a real surface, and so the heating differences for a finite catalytic surface in comparison with the fully catalytic surface would be less than shown in these figures. Note that a recently published study[10] also considered the effect of nonequilibrium flow over slender hypersonic vehicles with the same conclusion that substantial benefits for surfaces with low catalysis are recognized only in the nose dominated region of slender vehicles. The parametric nonequilibrium study of Ref. 10 was based on nose and body bluntness for a wide range of flow conditions.

Concluding Statements

A numerical study of several parameters that influence the heat transfer, drag, and shock-layer mass-flow rate on slender hypersonic vehicles was conducted. The calculations were performed with a viscous shock-layer code that has been demonstrated to yield excellent comparisons with flight- and ground-test data and the results of other detailed codes. The study focuses the attention of present-day designers of future high-performance hypersonic vehicles on fundamental parameters, such as bluntness (nose and cone angle) and angle of attack, which can affect even initial design and trajectory options. The influence of gas chemistry was also illustrated. The present information can be of practical use in the design of slender hypersonic vehicles. Results from the conditions considered by this study can be summarized as follows.

1) At zero incidence, nose blunting reduced laminar heating loads to the vehicles and decreased total drag. When transition was included, the benefit of nose blunting on heating and total drag increased significantly.

2) For the range of angles of attack and cone angles, the effect of increasing bluntness is to reduce the laminar heating levels and delay transition. The laminar and turbulent levels on the windward centerline were found to increase by a factor of 5 for the present cone angle and angle-of-attack range.

3) Laminar heating rates computed for an angle of attack were shown to be significantly higher than corresponding rates for an equivalent cone case. However, essentially the same levels were computed for turbulent flow. These conclusions were the same for an assumption of perfect-gas or equilibrium-air chemistry.

4) For calculations including transition at 0-deg angle of attack, the assumption of equilibrium-air chemistry was shown to increase the aerothermal loads and drag over corresponding perfect-gas calculations.

5) The integrated shock-layer mass-flow rate was demonstrated to increase significantly with angle of attack. The boundary-layer or gas chemistry condition and increasing nose bluntness were shown to have a relatively small influence on the mass-flow rate at a given angle of attack.

6) For these slender body studies, an incremental change in cone half-angle produced a significant effect on the aerodynamic and aerothermal results.

7) Calculations of the nonequilibrium flow over a slender blunted cone at 0-deg angle of attack showed that surface catalytic effects were significant only for a limited distance, which was primarily the nose-dominated region.

References

[1]Williams, R. M., "National Aerospace Plane: Technology for America's Future," *Aerospace America*, Vol. 24, No. 11, 1986, pp. 18–22.

[2]Martin, J. A., et al., "Special Section—Orbit-On-Demand Vehicle," *Aerospace America*, Vol. 23, No. 2, 1985, pp. 46–48.

[3]Vatsa, V. N, Thomas, J. L., and Wedan, B. W., "Navier-Stokes Computations of Computations of a Prolate Spheriod at Angle of Attack," *Journal of Aircraft*, Vol. 26, No. 11, 1989, pp. 986–993.

[4]Chakravarthy, S. R., Szema, K. Y., Goldberg, U. C., Gorski, J. J., and Osher, S., "Application of a New Class of High Accuracy TVD Schemes to the Navier-Stokes Equations," AIAA Paper 85-0165, 1985.

[5]Gnoffo, P. A., McCandless, R. S., and Yee, H. C., "Enhancements to Program LAURA for Computation of Three-Dimensional Hypersonic Flow," AIAA Paper 87-0280, 1987.

[6]Lawrence, S. L., Tannehill, J. C., and Chaussee, D. S., "An upwind Algorithm for the Parabolized Navier-Stokes Equations," AIAA Paper 86-1117, 1986.

[7]Thompson, R. A., Zoby, E. V, Wurster, K. E., and Gnoffo, P. A., "An Aerothermodynamic Study of Slender Conical Vehicles," AIAA Paper 87-1475, June 1987.

[8]Lee, K. P., Gupta, R. N., Moss, J. N., Zoby, E. V., and Tiwari, S. N., "Viscous Shock Layer Solutions for the Low Density Hypersonic Flow Past Long Slender Bodies," AIAA Paper 88-0460, Jan. 1988.

[9]Gupta, R. N., Lee, K. P., Moss, J. N., Zoby, E. V., and Tiwari, S. N., "Viscous Shock-Layer Analysis of Hypersonic Flows Over Long Slender Bodies," AIAA Paper 87-2487, Aug. 1987.

[10]Zoby, E. V., Lee, K. P., Gupta, R. N., Thompson, R. A., and Simmonds, A. L., "Viscous Shock-Layer Solutions with Nonequilibrium Chemistry for Hypersonic Flows Past Slender Bodies," AIAA Paper 88-2709, June 1988.

[11]Pugh, P. G., and Ward, L. C., "A Parametric Study of the Use of Nose Blunting to Reduce the Supersonic Wave Drag of Forebodies," Aeronautical Research Council, ARC-CP-1271, 1974.

[12]Ashby, G. C., Jr., and Harris, J. E., "Boundary-Layer Displacement-Thickness Effects on Zero-Lift Drag of a Series of Power-Law Bodies at Mach 6," NASA TN D-7723, Sept. 1974.

[13]Moeckel, W. E., "Some Effects of Bluntness on Boundary-Layer Transition and Heat Transfer at Supersonic Speeds," NACA Rept. 1312, 1957.

[14]Davis, R. T., "Numerical Solution of the Hypersonic Viscous Shock-Layer Equations," *AIAA Journal*, Vol. 8, Dec. 1970, pp. 2152–2156.

[15]Murray, A. L., and Lewis, C. H., "Hypersonic Three-Dimensional Viscous Shock Layer Flows Over Blunt Bodies," *AIAA Journal*, Vol. 16, No. 12, 1978, pp. 1279–1286.

[16]Thareja, R. R., Szema, K. Y., and Lewis, C. H., "Chemical Equilibrium Laminar or Turbulent Three-Dimensional Viscous Shock-Layer Flows," *Journal of Spacecraft and Rockets*, Vol. 20, No. 5, 1983, pp. 454–460.

[17]Swaminathan, S., Kim, M. D., and Lewis, C. H., "Three-Dimensional Nonequilibrium Viscous Shock-Layer Flows Over Complex Geometries," AIAA Paper 83-0212, Jan. 1983.

[18]Thompson, R. A., "Three-Dimensional Viscous-Shock-Layer Application for the Space Shuttle Orbiter," *Thermophysical Aspects of Re-entry Flows*, edited by J. N. Moss and C. D. Scott, *Progress in*

Astronautics and Aeronautics, Vol. 103, AIAA, New York, 1986, pp. 541–570.

[19]Thompson, R. A, "Comparisons of Nonequilibrium Viscous-Shock-Layer Solutions with Windward Surface Shuttle Heating Data," AIAA Paper 87-1473, June 1987.

[20]Cebeci, T., and Smith, A.M.O., *Analysis of Turbulent Boundary Layers*, Academic, New York, 1974., pp. 211-217.

[21]Beckwith, I. E., and Bertram, M. H., "A Survey of NASA Langley Studies on High-Speed Transition and the Quiet Tunnel," NASA TMX-2566, 1972.

[22]Dhawan, S., and Narashimha, R., "Some Properties of Boundary Layer Flow During Transition from Laminar to Turbulent Motion," *Journal of Fluid Mechanics*, Vol. 3, Pt 4, Jan. 1958, pp. 418–436.

[23]Muir, J. F., and Trujillo, A. A., "Experimental Investigation of the Effects of Nose Bluntness, Free-Stream Unit Reynolds Number, and Angle of Attack on Cone Boundary Layer Transition at a Mach Number of 6," AIAA Paper 72-216, Jan. 1972.

[24]Stainback, P. C., "Effect of Unit Reynold Number, Nose Bluntness, Angle of Attack and Roughness on Transition on a 5° Half-Angle Cone at Mach 8," NASA TN D-4961.

[25]Wright, R. L., and Zoby, E. V., "Flight Measurements of Boundary-Layer Transition on a 5° Half-Angle Cone at a Free-Stream Mach Number Of 20 (Re-entry F)," NASA TM X-2253, 1971.

[26]Stetson, K. F., and Rushton, G. H., "Shock Tunnel Investigation of Boundary-Layer Transition at $M=5.5$," *AIAA Journal*, Vol. 5, No. 5, 1967, pp. 899–906.

[27]Stetson, K. F., "Mach 6 Experiments of Transition on a Cone at Angle of Attack," *Journal of Spacecraft and Rockets*, Vol. 19, No. 5, 1982, pp. 387–403.

[28]Nowak, R. J., Albertson, C. W., and Hunt, L. R., "Aerothermal Tests of a 12.5° Cone at Mach 6.7 for Various Reynolds Numbers, Angles of Attack, and Nose Shapes," NASA TP 2345, Jan. 1985.

[29]Holden, M. S., "Experimental Studies of the Effects of Asymmetric Transition on the Aerothermal Characteristics of Hypersonic Blunted Slender Cones," AIAA Paper 85-325, Jan. 1985.

[30]Martellucci, A., and Neff, R. S., "The Influence of Asymmetric Transition on Re-Entry Vehicle Motion," AIAA Paper 70-987, Aug. 1970.

[31]Maddalon, D. V., and Henderson, A., Jr., "Hypersonic Transition Studies on a Slender Cone at Small Angles of Attack," *AIAA Journal*, Vol. 6. No. 1, 1968, pp. 176–177.

[32]Adams, J. C., Jr., "Implicit Finite-Difference Analysis of Compressible Laminar, Transitional, and Turbulent Boundary Layers Along the Windward Streamline on a Sharp Cone at Incidence," Arnold Engineering Development Center, Arnold AFS, Tullahoma, TN, AEDC-TR-71-235, Dec. 1971.

[33]Widhopf, G. F., "Turbulent Heat-Transfer Measurements on a Blunt Cone at Angle of Attack," *AIAA Journal*, Vol. 9, No. 8, 1971, pp. 1574–1580.

Clark H. Lewis
Associate Editor